Neurobiology of Disease

Acute Polyglutamine Expression in Inducible Mouse Model Unravels Ubiquitin/Proteasome System Impairment and Permanent Recovery Attributable to Aggregate Formation

Zaira Ortega,[1] Miguel Díaz-Hernández,[1] Christa J. Maynard,[2] Félix Hernández,[1] Nico P. Dantuma,[2] and José J. Lucas[1]

[1]Centro de Biologia Molecular "Severo Ochoa" (CBM"SO"), Consejo Superior de Investigaciones Científicas (CSIC), Universidad Autonoma de Madrid (UAM), and CiberNed, 28049 Madrid, Spain, and [2]Department of Cell and Molecular Biology, Karolinska Institutet, S-17177 Stockholm, Sweden

The presence of intracellular ubiquitylated inclusions in neurodegenerative disorders and the role of the ubiquitin/proteasome system (UPS) in degrading abnormal hazardous proteins have given rise to the hypothesis that UPS-impairment underlies neurodegenerative processes. However, this remains controversial for polyglutamine disorders such as Huntington disease (HD). Whereas studies in cellular models have provided evidence in favor of UPS-impairment attributable to expression of the N-terminal fragment of mutant huntingtin (N-mutHtt), similar studies on mouse models failed to do so. Furthermore, we have recently shown that the increase in polyubiquitin conjugates reported in the brain of N-mutHtt mice occurs in the absence of a general UPS-impairment. In the present study we aim to clarify the potential of N-mutHtt to impair UPS function *in vivo* as well as the mechanisms by which neurons may adapt after prolonged exposure to N-mutHtt in genetic models. By combining UPS reporter mice with an inducible mouse model of HD, we demonstrate for the first time polyglutamine-induced global UPS-impairment *in vivo*. UPS-impairment occurred transiently after acute N-mutHtt expression and restoration correlated with appearance of inclusion bodies (IBs). Consistently, UPS recovery did not take place when IB formation was prevented through administration of N-mutHtt aggregation-inhibitors in both cellular and animal models. Finally, no UPS-impairment was detected in old mice constitutively expressing N-mutHtt despite the age-associated decrease in brain proteasome activity. Therefore, our data reconcile previous contradictory reports by showing that N-mutHtt can indeed impair UPS function *in vivo* and that N-mutHtt aggregation leads to long lasting restoration of UPS function.

Introduction

Huntington disease (HD) is the most common of nine inherited neurological disorders caused by CAG triplet-repeat expansions in their respective genes (Orr and Zoghbi, 2007). The CAG-repeats encode expanded polyglutamine (polyQ) sequences that confer toxicity to the mutated proteins, and these diseases share the presence of intraneuronal inclusion bodies (IBs) that consist of the aggregation-prone polyQ proteins (Ross, 1997; Ross and Poirier, 2004).

The primary proteolytic machinery responsible for the turnover of proteins in the cytosol and nuclei of cells, including the destruction of misfolded or otherwise abnormal proteins, is the ubiquitin/proteasome system (UPS) (Hershko and Ciechanover, 1998). Deficient UPS function is believed to contribute to the etiology of Parkinson disease (Cook and Petrucelli, 2009), amyotrophic lateral sclerosis (Cheroni et al., 2009), and prion-diseases (Kristiansen et al., 2007) but remains controversial regarding PolyQ-disorders (Davies et al., 2007; Ortega et al., 2007).

A number of studies in cellular models have provided evidence in favor of UPS impairment caused by expression of the N-terminal fragment of mutant-huntingtin (N-mutHtt) (Bence et al., 2001; Jana et al., 2001; Bennett et al., 2005; Duennwald and Lindquist, 2008; Mitra et al., 2009). However, similar studies on mouse models failed to detect UPS impairment either by measuring proteasome activity in brain extracts (Diaz-Hernandez et al., 2003; Bett et al., 2006) or by using UPS reporter mice that express specifically designed proteasome substrates (Bett et al., 2009; Maynard et al., 2009). Moreover, we have recently shown that the increase in polyubiquitin conjugates in the brain of R6/2 mice (Bennett et al., 2007) occurs in the absence of a general UPS impairment (Maynard et al., 2009).

In the present study we aim to clarify the potential of PolyQ to impair UPS function *in vivo* as well as the mechanisms by which neurons may adapt. We suggest two reasons by which PolyQ-induced impairment of the UPS might have gone unnoticed in *in vivo* studies. The first is related to the fact that the R6 mouse models (Mangiarini et al., 1996) used in previous UPS studies show an early onset phenotype and die prematurely and to the fact that brain proteasome activity decreases with aging (Keller et al., 2000a), which itself has been linked to the late onset of HD (Zhou et al., 2003). The second is related to the possibility of

Received Nov. 16, 2009; revised Jan. 12, 2010; accepted Jan. 22, 2010.

This work was supported by the Spanish Ministry of Science/MEC, CiberNed, Comunidad Autónoma de Madrid, Fundación "La Caixa," and Fundación Ramón Areces (to J.J.L.); the HighQ Foundation (to J.J.L. and N.P.D.); the Swedish Research Council and the Nordic Center of Excellence Neurodegeneration; the Swedish Cancer Society, the Hereditary Disease Foundation, the Marie Curie Research Training Network (MRTN-CT-2004-512585), and the Karolinska Institute (to N.P.D.). We thank members of the Lucas laboratory for helpful suggestions. We also thank Owen Howard for style correction and Desireé Ruiz and Alicia Tomico for excellent technical assistance.

Correspondence should be addressed to José J. Lucas, Centro de Biología Molecular "Severo Ochoa," CSIC/UAM y CiberNed, c/ Nicolas Cabrera, 1, 28049 Madrid, Spain. E-mail: jjlucas@cbm.uam.es.

DOI:10.1523/JNEUROSCI.5673-09.2010

 0270-6474/10/303675-14$15.00/0

gradual adaptive changes secondary to long-lasting exposure to N-mutHtt in genetic models, such as the protective IB formation recently proposed in cell models (Mitra et al., 2009).

HD94 mice are inducible (Yamamoto et al., 2000) and have a milder phenotype than R6 mice and an almost normal lifespan (Diaz-Hernandez et al., 2005). We therefore decided to combine them with UPS reporter mice (UbGFP) (Lindsten et al., 2003) to (1) analyze them at advanced stages, once an age-dependent decrease in proteasome activity should have taken place, and (2) explore whether transient UPS impairment could be detected *in vivo* in adult brain after acute N-mutHtt expression and, in such a case, explore the adaptive mechanism by which UPS function normalizes.

Materials and Methods

Animals. Mice: previously described HD94 (Yamamoto et al., 2000), R6/1 (Mangiarini et al., 1996), and UbGFP-line1 (Lindsten et al., 2003) mice were bred at Centro de Biología Molecular "Severo Ochoa" animal facility. Mice were housed five per cage with food and water available *ad libitum* and maintained in a temperature-controlled environment on a 12/12 h light/dark cycle with light onset at 07:00 A.M. All experiments were performed in accordance with institutional guidelines approved by the ethical committee of Consejo Superior de Investigaciones Científicas (CSIC). UbGFP:HD94 mice result from the breeding of the double transgenic mice tTA+UbGFP, obtained from the breeding of CaMKIIα-tTA mice (Mayford et al., 1996) with UbGFP-line1 mice (Lindsten et al., 2003), with TetO mice (carrying the bidirectional tet-responsive promoter followed by a chimeric mouse/human exon 1 with a polyQ expansion of 94 repeats) (Yamamoto et al., 2000). UbGFP:R6/1 mice result from the breeding of R6/1 mice (Mangiarini et al., 1996) with UbGFP-line1 mice (Lindsten et al., 2003).

Doxycycline treatment. UbGFP:HD94 mice and their control littermates were given doxycycline (Sigma-Aldrich) (0.5 g/L) in drinking water *ad libitum* for 8 or 12 weeks from embryonic day 16. This paradigm was chosen based on our previous observation that it results in full shutdown of transgene expression in the same conditional mouse model of Huntington disease (Diaz-Hernandez et al., 2005).

Riluzole treatment. Riluzole (1.2 g/L or 2 g/L) (Sigma-Aldrich) was complexed with hydroxypropyl-β-cyclodextrin (Sigma-Aldrich) in water (4.5% w/v) and administered in light-protected drinking bottles. UbGFP:HD94 mice after 3.5 weeks of transgene expression or 3-week-old R6/1 mice were given riluzole for 3 d, either at 1.2 g/L for all 3 d or at 2 g/L for the first day and then at 1.2 g/L for the remaining 2 d (in view of the hypoactivity induced by 2 g/L riluzole when it was given for >1 d). Control mice were given 4.5% w/v hydroxypropyl-β-cyclodextrin.

Stereotaxic injection. Five 18-month-old UbGFP male mice received bilateral intrastriatal injections with lactacystin in one hemisphere and with vehicle (water) in the other hemisphere. Mice were anesthetized with isoflurane (1-chloro-2,2,2-trifluoroethyl-difluoromethylether) (Inibsa) diluted in a 50% O_2/50% NO_2 mixture. Mice were kept under anesthesia during the surgery with the aid of a gas mask. The scalp was incised along the midline, and two holes were made at the appropriate stereotaxic coordinates (mediolateral, 1.5 mm; anteroposterior, 0.5 mm; dorsoventral, 1.2 mm) according to the atlas of Paxinos and Franklin (2001). Intrastriatal administration of 2 μl of lactacystin at 10 μg/μl (right side) and 2 μl of distilled H_2O (left side) was performed using a 10 μl Hamilton syringe. Lactacystin and H_2O were infused at a rate of ~1 μl/min. After the injection, the needle was kept for additional 2 min and then slowly withdrawn.

Tissue preparation. In all experiments, wild-type and transgenic animals were processed in parallel and have been treated identically. Briefly, mice were killed by CO_2, and brains were removed and halved sagittally immediately after decapitation. Hemispheres were fixed with 4% paraformaldehyde in Sorensen phosphate buffer (PFA) overnight at 4°C, and then were either embedded in 3.5% bacteriological agar in distilled H_2O [brains for green fluorescent protein (GFP)-fluorescence study], or immersed in 30% sucrose in PBS for 48 h for cryoprotection and then in OCT (Optimal Cutting Temperature, Tissue-Tek) (brains for immunofluorescence or immunohistochemistry). Hemispheres were serially cut into 30 μm slices, using either a vibratome (Vibratome 1500) (for GFP-fluorescence study) or a freezing microtome (Leica) (cryoprotected hemispheres for immunofluorescent and immunohistochemical analysis), and placed in a solution containing 30% glycerol, 30% ethyleneglycol, 30% dH_2O, and 10% phosphate buffer at pH 7.2.

GFP-fluorescence, immunofluorescence, and immunohistochemistry. For GFP-fluorescence detection, slices were transferred to slides, incubated with Hoechst 33342 (DAPI) (Biologics) (2.5 μg/ml) for 10 min, and then air dried in darkness and coverslipped with Fluorosave. Immunofluorescence staining was performed pretreating free-floating slices with 0.1% Triton X-100 for 15 min and glycine 1 M for 30 min at room temperature, followed by blocking solution (1% BSA and 0.1% Triton X-100) for 1 h. Next, slices were incubated for 2 h at room temperature with primary antibodies at the following dilutions: anti-GFP (rabbit, Invitrogen), anti-NeuN (mouse, Millipore Bioscience Research Reagents), anti-GFAP (rabbit, Promega), anti-CNPase (rabbit, Abcam), anti-iba1 (rabbit, Wako), anti-β-galactosidase (rabbit, ICN Biomed.-Cappel), and anti-N-terminal htt (mouse MAB5374, Millipore Bioscience Research Reagents). Then the sections were washed in PBS and incubated with secondary antibodies for 1 h (1:200) goat anti-rabbit TexasRed-conjugated (Invitrogen), goat anti-mouse TexasRed-conjugated (Invitrogen), goat anti-rabbit TexasRed-conjugated (Invitrogen), and goat anti-mouse OregonGreen-conjugated (Invitrogen). Finally, nuclei were stained by using DAPI (Biologics) (2.5 μg/ml) for 10 min, and then sections were air dried in darkness and coverslipped with Fluorosave. For immunohistochemistry, free-floating sections were pretreated for 30 min in 1% H_2O_2/PBS, followed by 1 h with 1% BSA, 5% FBS, and 0.2% Triton X-100; and then incubated overnight at 4°C with primary antibody at the following dilutions: anti-β-galactosidase (ICN Biomed.-Cappel; 1:5000); anti-GFP (Invitrogen; 1:5000); anti-N-terminal htt (MAB5374, Millipore Bioscience Research Reagents; 1:200); anti-cleaved caspase3 (Cell Signaling Technology; 1:50). Next, slices were incubated with avidin-biotin complex (Elite Vectastain kit, Vector Laboratories). Chromogen reactions were performed with diaminobenzidine (SIGMA*FAST* DAB, Sigma-Aldrich) and 0.003% H_2O_2 for 10 min. Finally, sections were coverslipped with Fluorosave.

Primary neuron culture and transfection. Primary neuronal cultures were prepared according to modifications of established procedures (Huettner and Baughman, 1986; Dubinsky, 1989; Martin-Aparicio et al., 2001). Pups were killed at embryonic day 18. Embryo cortices and striata were dissected and dissociated with the Papain Dissociation System (Worthington). Cortical and striatal neurons were maintained in Neurobasal medium (Invitrogen) supplemented with 1% sodium pyruvate, 0.5 mM glutamine, 10% v/v horse serum, and 1% penicillin/streptomycin, and grown on 3 μg/ml laminin (Sigma) and 10 μg/ml poly-L-lysine-coated open μ-Slide with eight wells (chamber slide) for high quality microscopy (Ibidi). After 2 h of incubation, the culture medium was replaced with a Neurobasal medium supplemented with 1% sodium pyruvate, 0.5 mM glutamine, 2% B27. Cells were maintained in 95% air/5% CO_2 in a humidified incubator at 37°C. For inhibition of proteasome activity, neuronal cultures were adjusted to 50 μM MG-132 (Calbiochem). For inhibition of aggregation, neuronal cultures were adjusted to 400 μM PGL-135 or 40 μM riluzole. In both treatments, drugs were added 1 h after transfection, and primary cultures were incubated for an additional 16 to 24 h. Control cells were incubated with an equivalent amount of solvent, H_2O in the case of MG-132, DMSO in the case of PGL-135 (up to 0.3% final concentration), and cyclodextrin in the case of riluzole (6.75×10^{-3} w/v final concentration).

Transfection was performed 1 d after plating. Cells were transiently transfected with 1 μg DNA and 3 μl Lipofectamine (Invitrogen) in 100 μl Neurobasal medium. The mixture was carefully (drop by drop) directly added to the medium (without antibiotics) and incubated for 2 h in 95% air/5% CO_2 in a humidified incubator at 37°C. Next, cells were washed three times with PBS and added to Neurobasal medium supplemented with 1% sodium pyruvate, 0.5 mM glutamine, 2% B27, and 1% penicillin/streptomycin. Transfection efficiency was controlled by counting the number of transfected neurons corrected by the total number of neurons (a minimum of 300 cells were analyzed per experimental condition). Transfection efficiency was between 3% and 6% across all experiments.

Robotic microscope imaging system and image analysis. For immunohistochemistry analysis, Axioskop2 plus microscope and a CCD camera (Coolsnap FX color) was used. For fluorescence detection, an inverted Axiovert200 (Zeiss) microscope was used. Plan-Apochromat 10× (numerical aperture 0.45), 20× (numerical aperture 0.6), and 40× objectives were used. Xenon lamp XBO (75W/2) illumination was supplied by a liquid light guide to reduce electrical noise. Images were detected and digitized with a Hamamatsu C9100-02 digital camera and Universal Imaging MetaMorph software.

Stage movements and focusing were executed with computer-controlled stepper motors. Fluorescence excitation and emission filters [GFP: 473-498, 552-577 86007bs; cyan fluorescent protein (CFP): 426-446/422-432, 455 dichroic long-pass, 460-500; yellow fluorescent protein (YFP): 490-510, 510-560, HQ520LP; and DAPI: 359-371, 450LP] were moved into or out of the optical path with each program loop by two filter wheels (Sutter Instruments) under computer control. The whole system is mounted on a vibration isolation table to reduce noise. Computer commands that perform and coordinate automated stage movements, filter wheel movements, and focusing were generated with software programs that combine custom-designed and commercially available algorithms.

For analysis of transfected primary neurons, wells were scanned and images were taken once every 2 h (from 16 h to 24 h after transfection) to avoid photobleaching. The exposure time (70 milliseconds) and the sensitivity (30) were the same for YFP and CFP fluorescence and among experiments. Neurons were maintained in 95% air/5% CO_2 in a humidified incubator at 37°C between images. Measurements of CFP and YFP fluorescence were extracted from files generated with automated imaging by automated analysis software (ImageJ). CFP and YFP fluorescence was estimated by measuring fluorescence intensity over a region of interest that corresponded to the cell soma. These CFP and YFP intensity values were background-subtracted by using an adjacent area of the image. We classify neurons in increase or decrease of YFP fluorescence when the final fluorescence intensity increases or decreases in >50% respect to the initial fluorescence intensity respectively.

For analysis of GFP-positive cells on brain sections, 30 μm sagittal sections spanning the whole striatum (taken 120 μm apart) were entirely scanned and photographed. GFP fluorescence intensity over a region of interest that corresponds to a cell soma (based on roundness and size) was extracted from files generated with automated imaging by automated analysis software (ImageJ) and background-subtracted by using an adjacent area of the image. We classify neurons as positive for increased GFP fluorescence when its fluorescence intensity is >50% over background.

TUNEL assay. Mice were anesthetized and transcardially perfused with 4% PFA in PBS for 10 min. Brains were postfixed in 4% PFA for 2 h at 4°C and cryoprotected. Sections were treated following the protocol of the *In Situ* Cell Death Detection Kit, POD (Roche).

Filter trap assay. Hemibrains from vehicle- or riluzole-treated mice Ub-GFP:R6/1 ($n = 5$ for each genotype) were used to perform filter trap assay. The isolation of nuclei from total brain and the preparation of aggregates were performed as previously described (Davies et al., 1999). The cellulose acetate filters were incubated with the MAB5374 anti-N-terminal htt antibody (mouse, Millipore Bioscience Research Reagents) at 4°C overnight in 5% nonfat dried milk. A secondary goat anti-mouse immunoglobulins/HRP (DAKO; 1:1000), followed by ECL detection reagents (PerkinElmer), was used for immunodetection.

Purification of IBs by magnetic sorting and analysis in flow cytometer. Huntingtin-containing IBs from vehicle- or riluzole-treated UbGFP:R6/1 mice were obtained as previously described (Diaz-Hernandez et al., 2006). Briefly, brains were split along the midline, and one hemibrain of each animal was homogenized in a glass homogenizer with 6 ml of cold buffer 1 (10 mM Tris, 1 mM EGTA, 0.15 M NaCl, 10% sucrose, 0.1% Triton X-100; and protease inhibitors: 2 mM phenylmethylsulfonyl fluoride; 10 μg/ml aprotinin; 10 μg/ml leupeptin; and 10 μg/ml pepstatin). After centrifugation at 27,000 × *g* for 20 min at 4°C, the supernatant (S1) containing cytosol and organelles was discarded and the pellet (P1) containing IBs was again homogenized in buffer 2 (10 mM Tris, 1 mM EGTA, 0.15 M NaCl, 10% sucrose; and protease inhibitors: 2 mM phenylmethylsulfonyl fluoride; 10 μg/ml aprotinin; 10 μg/ml leupeptin; and 10 μg/ml pepstatin), before it was centrifuged again at 27,000 × *g* for 20 min. Pellet P2 was resuspended in 12 ml of buffer 2 and filtered through a 30-μm-diameter pore filter. The F1 filter fraction was then centrifuged at 27,000 × *g* for 20 min, and the resulting pellet P3 containing the huntingtin-containing IBs was resuspended in 2 ml of buffer 2. The IBs were then selected by magnetic sorting. For this, resuspended pellet P3 was incubated at 37°C for 1 h with a mouse monoclonal antibody against N-terminal htt (MAB5374; 1:200). After two rounds of centrifugation and resuspension in buffer 2, the IBs were incubated at 37°C for 1 h with rat anti-mouse IgG1 antibodies labeled with microbeads. The IBs labeled with microbeads were then retained on a column by a magnetic field, while the unlabeled material passed through. Finally, the magnetic field was removed from the column and the retained IBs were eluted with 750 μl of buffer 2 and stored at −70°C until their use in further analysis. Finally, 30 μl of each sample were taken to a final 100 μl volume with PBS and analyzed on a FACsCalibur flow cytometer (BD Biosciences) using CellQuest software (BD Biosciences).

Western blot analysis. Extracts for Western blot analysis from cultures were prepared by homogenizing cells in loading-buffer (50 mM Tris-HCl, pH 6.8, 100 mM dithiothreitol, 2% SDS, 0.1% bromophenol blue, 10% glycerol), and boiled for 5 min. Extracts for Western blot analysis from mouse brain were prepared by homogenizing the brain areas in ice-cold extraction buffer consisting of 20 mM HEPES pH 7.4, 100 mM NaCl, 20 mM NaF, 1% Triton X-100, 1 mM sodium orthovanadate, 5 mM EDTA, and protease inhibitors (2 mM PMSF, 10 μg/ml aprotinin, 10 μg/ml leupeptin, and 10 μg/ml pepstatin). The samples were homogenized and centrifuged at 15,000 × *g* for 20 min at 4°C. The resulting supernatant was collected, and protein content was determined by Bradford. Total protein (15 μg) was electrophoresed on 12% SDS-PAGE gel and transferred to a nitrocellulose membrane (Schleider and Schuell). The filters were incubated with the antibodies anti-N-terminal htt (mouse, Millipore Bioscience Research Reagents), anti-GFP (mouse, Santa Cruz Biotechnology) and anti-β-actin (mouse, Sigma-Aldrich), at 4°C overnight in 5% nonfat dried milk. A secondary goat anti-mouse immunoglobulins/HRP (DAKO; 1:1000), followed by ECL detection reagents (PerkinElmer), was used for immunodetection.

Proteasome activity assays. Mice were killed by CO_2, and brains were removed. Brains were quickly dissected on an ice-cold plate. Striatal tissue was homogenized in extraction buffer (10 mM Tris-HCl, pH 7.8, 0.5 mM dithiothreitol, 5 mM ATP, 0.03% Triton X-100, and 5 mM $MgCl_2$). Lysates were centrifuged at 13,000 × *g* at 4°C for 20 min, and the resulting supernatants were placed on ice and assayed for protein concentrations by the Bradford method (Bio-Rad). For determination of proteasome activity, extracts were adjusted to 0.5 mg/ml total protein by dilution with extraction buffer. All assays were done in triplicate. Chymotrypsin-like activity was determined using the substrate Suc-LLVY-aminomethylcoumarin (AMC) (Sigma; 50 μM), and caspase-like activity was determined using the substrate Z-LLE-β-2-naphthylamine (Nap) (Sigma; 0.2 mM). Assay mixtures containing 10 μg of protein, substrate, and 50 mM HEPES–KOH, pH 7.5, are made up in a final volume of 400 μl. Incubations were performed at 37°C for 30 and 60 min. The cleavage products AMC and Nap were analyzed, after stopping the reaction with 1 ml of 10% SDS, in a fluorimeter (excitation/emission: 335/410 nm for Nap and 380/460 nm for AMC). Product formation was linear with time (at least for 60 min). Background activity (caused by nonproteasomal degradation) was determined by addition of the proteasome inhibitor lactacystin at a final concentration of 50 μM (Sigma) or MG-132 at a final concentration of 10 μM (Calbiochem).

Quantitative reverse transcription-PCR. Mouse tissue RNA samples ($n = 5$ for UbGFP mice and $n = 7$ for UbGFP:HD94 mice in the experiment of acute N-mutHtt expression, and $n = 7$ for UbGFP mice and $n = 6$ for R6/1 mice in the experiment with riluzole treated mice) were analyzed for expression of the corresponding transgenes and uniformity across replicates. For each replicate, the striatum was dissected and RNA extracted with Qiagen RNeasy Protect kit (Qiagen). RNA was quantified in a Nanodrop ND-1000 spectrophotometer (Thermo Fisher Scientific). All samples showed 260/280 ratio values around 2, which corresponds to pure RNA. Yield range was between 70 and 300 ng/μl. RNA Integrity was

checked with the Agilent 2100 Bioanalyzer. RIN values were between 7.10 and 8.30 showing good integrity. Reverse transcription (RT) reactions were performed with High Capacity RNA-to-cDNA Master Mix with No-RT Control (Applied Biosystems PN 4390712). One microgram of total RNA from each sample was combined with 4 μl of master mix (includes a mixture of random primers and oligo-dT for priming). Reaction volume was taken to 20 μl with DNase/RNase free distilled water (Invitrogen). Thermal steps: 5′ × 25°C, 30′ × 42°C, and 5′ × 85°C. RT-amplifications were either negative or delayed >5 cycles compared to the corresponding RT+ reactions. Intron-spanning (β-actin) and non-intron-spanning (18S and GAPDH) assays were designed using Probe Finder software (Roche Applied Science). Primers for UbGFP transgene: 5′-GGGCACAAGCTGGAGTACAAC-3′ and 5′-GATGCCGTTC-TTCTGCTTGTC-3′. Primers for N-mutHtt: 5′-CGGCTGAGGCAG-CAGCGGCTGT-3′ and 5′-GCAGCAGCAGCAGCAACAGCCGCCA-CCGCC-3′. qPCR reactions were performed in triplicates in 10 μl final volume with the cDNA amount equivalent to 5 ng of total RNA, 250 nM of each primer, and 5 μl of Power Sybr Green PCR Master Mix (Applied Biosystems PN 4367659), which includes AmpliTaq Gold DNA Polymerase. For 18S, GAPDH, β-actin, and UbGFP genes we performed an initial denaturation of 10′ × 95°C followed by 40 two-step cycles (15′ × 95°C + 1′ × 60°C). We also included a melting curve from 60 to 95°C (2% ramp) at the end of the program to verify the specificity of the PCR. Fluorescence was acquired during the 60°C and melting steps. For N-mutHtt, the second step consisted of 34 four-step cycles (30′ × 94°C + 30′ × 68°C + 1′30′ × 72°C + 15′ × 82.6°C). Fluorescence was acquired during the 82.6°C step to avoid coquantification of a secondary peak with a smaller Tm that was detected in the melting curve. SDS 2.2.1 (Applied Biosystems) was used for data analysis. To normalize the data respect to the three control genes (18S, β-actin and GAPDH) two algorithms included in the program Genex (NormFinder and GeneNorm) were used.

Data analysis. In all *in vivo* experiments, at least six animals per group were analyzed and data are presented as mean ± SEM. Significant differences between the groups were evaluated using Student *t* test in the case of parametric population, and Mann–Whitney test in the case of nonparametric populations. In all experiments performed in primary cultures, at least 300 transfected neurons were analyzed. Significant differences between groups in culture experiments were evaluated using two-proportion comparison test.

Results

The Ub^{G76V}-GFP reporter does not accumulate in brain of late symptomatic HD94 mice despite age-associated decrease in brain proteasome activity

UbGFP mice that ubiquitously express the ubiquitin fusion degradation (UFD) substrate ubiquitin^{G76V}-green fluorescent protein (Ub^{G76V}-GFP) (Lindsten et al., 2003) were crossed with the inducible HD94 mouse model that expresses N-mutHtt in forebrain neurons in a tetracycline-repressible manner (HD94) (Yamamoto et al., 2000). UbGFP:HD94 mice with constitutive expression of N-mutHtt from birth (i.e., without any tetracycline administration) were analyzed at increasing ages at 2 month intervals from presymptomatic 2-month-old mice to early symptomatic 12-month-old mice. In good agreement with our previous report using symptomatic R6/1 and R6/2 mice (Maynard et al., 2009), no accumulation of the UPS impairment-reporter protein was observed in striatum, nor in any other brain region at any of the presymptomatic to early-symptomatic analyzed ages. As an example, histological analysis of native GFP fluorescence (Fig. 1*A*) and Western blot analysis (Fig. 1*H*) in the striatum of the Ub^{G76V}-GFP reporter protein is shown for 4-month-old UbGFP:HD94 mice. Figure 1*B* shows the presence of IBs in striatum of 4-month-old UbGFP:HD94 mice. The HD94 mouse phenotype, however, progresses from 12 months to death around the age of two years (Diaz-Hernandez et al., 2005). Additionally, proteasome activity is known to decrease with aging in the mouse brain (Keller et al., 2000a; Keller et al., 2000b; Zhou et al., 2003), and this has been linked to the late onset of HD (Zhou et al., 2003). In this regard, proteasome activity assays in striatal homogenates from control mice verified that an age-associated decrease in proteasome activity has indeed taken place by the age of 18 months (Fig. 1*G*). Accordingly, we also analyzed UbGFP:HD94 mice from 12 months, at 3 months intervals until late symptomatic, almost terminal stage at 21 months, and no accumulation of the Ub^{G76V}-GFP reporter protein could be detected in these mice (see Fig. 1*C*,*H–I* for examples of 18-month-old mice by native GFP fluorescence and Western blot analysis, respectively). Figure 1*D* shows the abundance of IBs in striatum of 18-month-old UbGFP:HD94 mice).

To fully validate this finding of no accumulation of the Ub^{G76V}-GFP reporter protein in UbGFP:HD94 mice that were both late symptomatic and of advanced age, expression and functionality of the reporter transgene was confirmed in 18-month-old UbGFP reporter mice by stereotaxic intrastriatal injection of the proteasome inhibitor lactacystin. As shown in Figure 1*E*, pharmacological proteasome inhibition resulted in a robust 875.3 ± 6.7% ($n = 5$; $p < 0.0001$) increase in the number of neurons accumulating the Ub^{G76V}-GFP reporter protein in 18-month-old UbGFP reporter mice. As expected, the density of UbGFP reporter-positive cells decreased as a factor of the distance to the site of lactacystin injection. However, the areas of striatum showing an at least 40% decrease in chymotrypsin activity still showed a significant increase in the number UbGFP reporter-positive cells (supplemental Fig. 1, available at www.jneurosci.org as supplemental material). Double labeling by immunofluorescence detection with specific marker antibodies for the different neural cell populations (Fig. 1*F*,*J*) verified expression of the Ub^{G76V}-GFP reporter transgene in all cell types. More precisely, 31.8% ± 5% of the Ub^{G76V}-GFP-positive cells were positive for the neuronal marker NeuN, 41.4% ± 4.8% were positive for the microglial marker Iba1, 7.0% ± 0.3% were positive for the astrocytic marker GFAP, and 19.6% ± 2.2% were positive for the oligodendrocyte marker CNPase (Fig. 1*J*). In summary, despite functional expression of the Ub^{G76V}-GFP reporter and an age-associated decrease in proteasome activity in striatal homogenates, no accumulation of the reporter protein could be detected in late symptomatic and old UbGFP:HD94 mice.

Transient accumulation Ub^{G76V}-GFP reporter after acute N-mutHtt expression

The above described absence of accumulation of the Ub^{G76V}-GFP reporter in aged HD94 mice, together with recent reports of no accumulation of this (Maynard et al., 2009) and of a similar (Bett et al., 2009) reporter of UPS impairment in R6 mice, suggest that there is no general UPS impairment in HD mouse brain despite the abundance of ubiquitylated IBs. However, the recently reported correlation of IB formation with recovery of UPS function in a cell model of HD (Mitra et al., 2009) prompted us to investigate whether acute expression of N-mutHtt in adult mouse brain would result in UPS reporter accumulation during the interval between the onset of N-mutHtt expression and IB formation. To test this, UbGFP:HD94 mice were maintained in N-mutHtt gene-off status by doxycycline administration during their entire embryonic life, and from birth to the age of 2 months. Doxycycline was then removed to allow expression of the N-mutHtt transgene, and mice were analyzed at different time intervals up to 24 weeks after induction of N-mutHtt expression (Fig. 2*A*). To

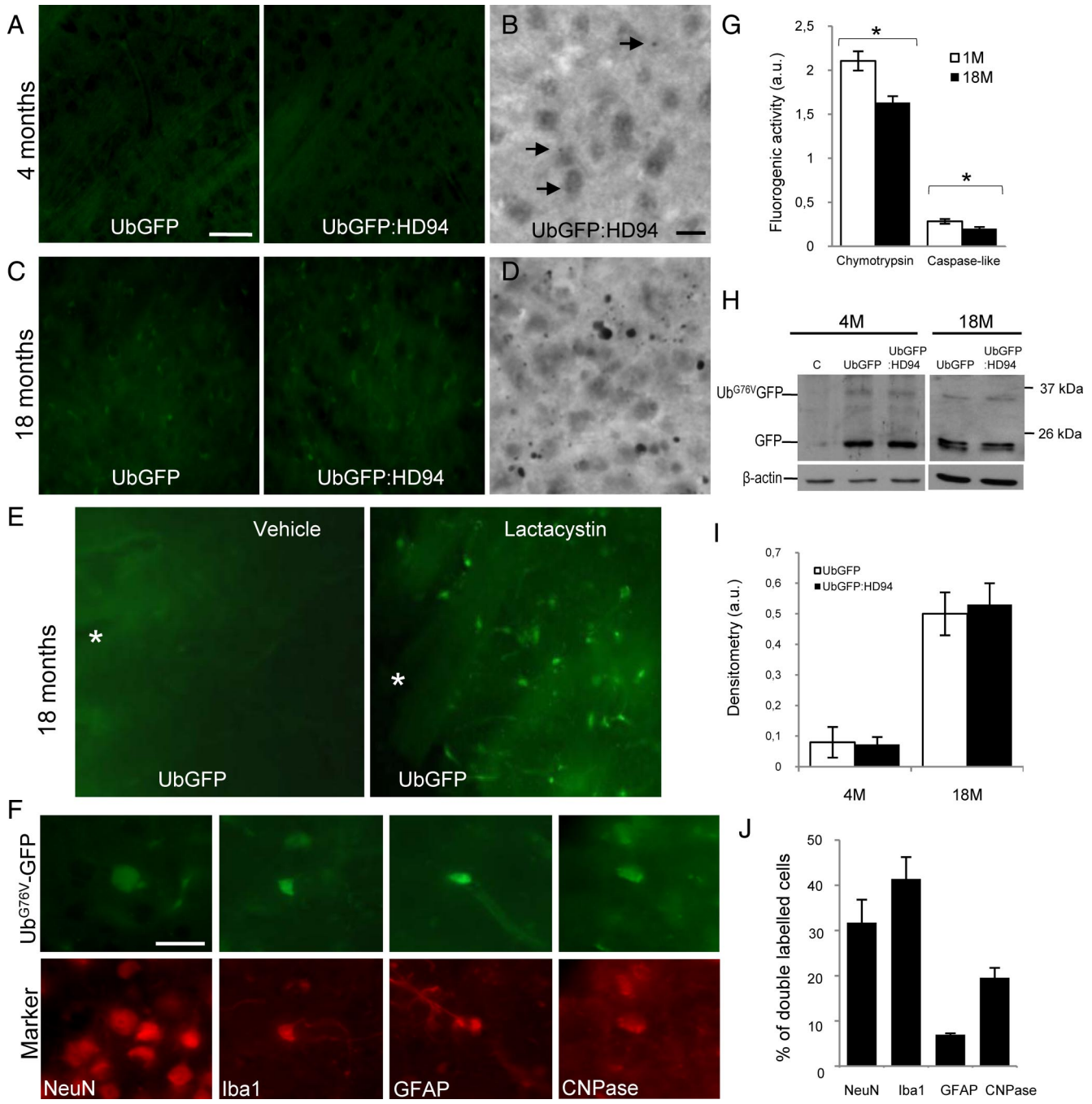

Figure 1. Absence of UPS reporter protein accumulation in UbGFP:HD94 mice even after age-associated decrease in UPS activity. ***A***, ***C***, GFP-fluorescence detection in striatal sagittal sections from 4-month-old (***A***) or 18-month-old (***C***) UbGFP and UbGFP:HD94 mice. Scale bar in ***A*** corresponds to 50 μm in ***A*** and ***C***. ***B***, ***D***, Immunohistochemistry with anti-N-terminal huntingtin antibody in striatal sagittal sections from 4-month-old (***B***) and 18-month-old (***D***) UbGFP:HD94 mice. Arrows indicate IBs. Scale bar in ***B*** corresponds to 10 μm in ***B*** and ***D***. ***E***, GFP-fluorescence detection in striatal sagittal sections from 18-month-old UbGFP mice intrastriatally injected with 2 μl of vehicle (water) or 2 μl of a 10 μg/μl lactacystin solution. * indicates the trajectory of the needle. ***F***, GFP-positive cells were also labeled by immunofluorescence with neuron (NeuN), microglia (iba1), astrocyte (GFAP), and oligodendrocyte (CNPase) marker antibodies in sections from 18-month-old UbGFP mice intrastriatally injected with lactacystin. Scale bar, 20 μm. ***G***, Chymotrypsin-like and caspase-like peptidase activities of the proteasome (by determining cleavage of the fluorogenic substrates SUC-LLVY-AMC and Z-LLE-β-NAP, respectively) assayed in striatal extracts from 1- or 18-month-old control mice. Proteasome activity is normalized by assaying the same amount of striatal tissue (10 μg) in each sample. ***H***, Western blot showing the full-length reporter construction (Ub^{G76V}-GFP) and the truncated form (GFP), in the St of 4- or 18-month-old wild-type (***c***), UbGFP, and UbGFP:HD94 mice. ***I***, Histogram showing the densitometric quantification [in arbitrary units (a.u.)] of Western blot detected Ub^{G76V}-GFP corrected by β-actin in 4- or 18-month-old UbGFP and UbGFP:HD94 mice. ***J***, Histogram showing the average percentage of GFP-positive cells that are neurons (NeuN), microglia (Iba1), astrocytes (GFAP), or oligodendrocytes (CNPase), in sections from 18-month-old UbGFP mice intrastriatally injected with lactacystin. Data are presented as mean ± SEM. *$p < 0.05$; ***$p < 0.001$.

monitor the rate of transgene induction, we performed immunohistochemical analysis of the β-gal reporter, which is expressed bicistronically with N-mutHtt and can be detected with higher sensitivity (Yamamoto et al., 2000; Martin-Aparicio et al., 2001) than N-mutHtt itself. As shown in Figure 2, *B* and *C*, striatal transgene expression was detectable after 1 week of doxycycline removal, growing exponentially after the second week, finally reaching a plateau after 16 weeks of expression.

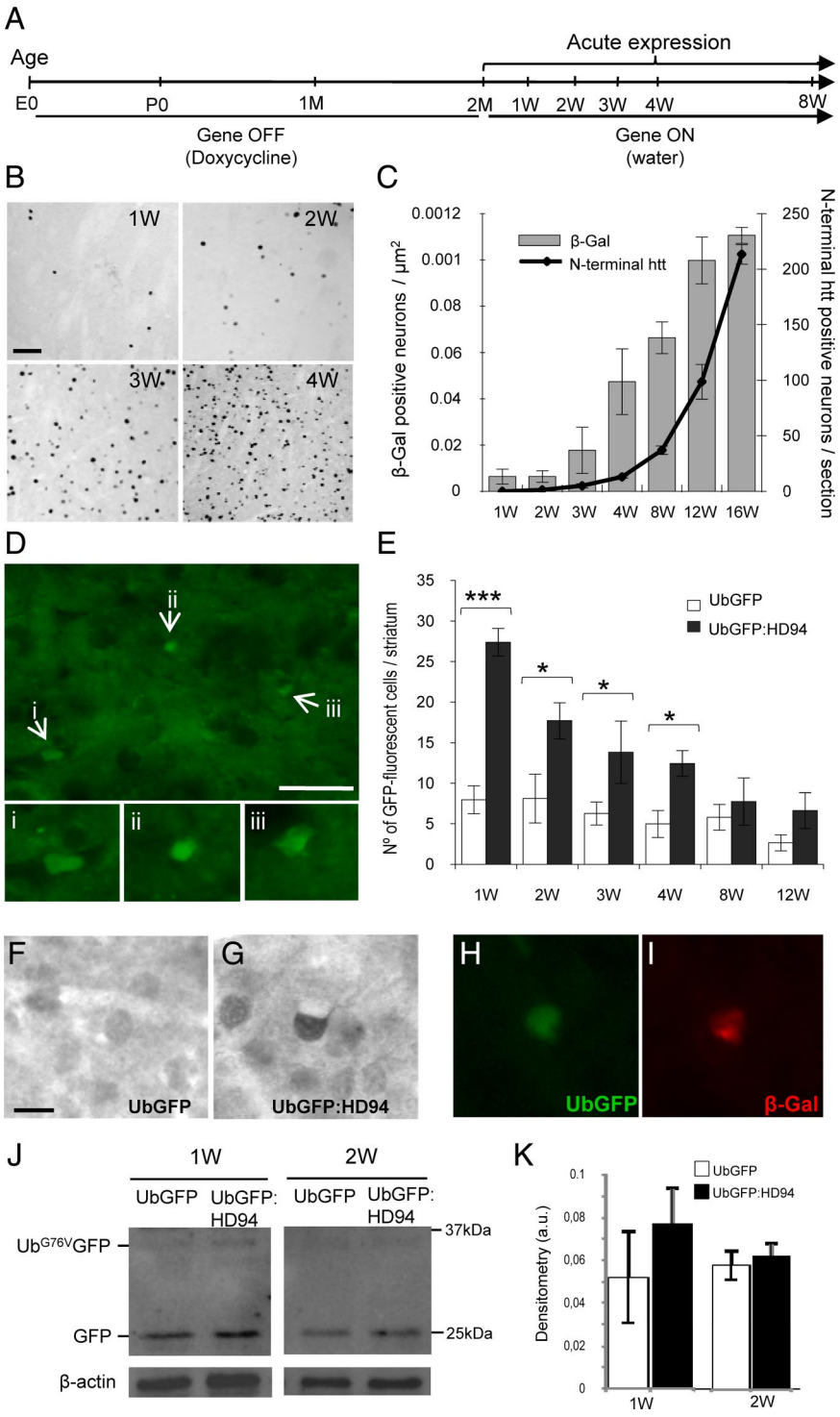

Figure 2. Transient UPS reporter protein accumulation in UbGFP:HD94 mice with acute expression of N-mutHtt. ***A***, Diagram showing the doxycycline administration protocol for acute expression of N-mutHtt in 2-month-old UbGFP:HD94 mice. Doxycycline was given to the mice in drinking water starting at embryonic day 0 (E0) by giving it first to the mothers, and it was then maintained from birth (P0) to 2 months (2M) of age. Mice were then analyzed weekly for 4 weeks and then every 4 weeks up to 24 weeks after doxycycline removal. ***B***, Immunohistochemical detection of β-gal in striatal sagittal sections from UbGFP:HD94 mice after 1, 2, 3, and 4 weeks of doxycycline removal. Scale bar, 100 μm. ***C***, Histogram showing the number of β-gal-immunoreactive (bar chart) or N-mutHtt-immunoreactive (line chart) neurons per μm^2 in striatal sagittal sections from UbGFP:HD94 mice after 1 to 16 weeks of N-mutHtt expression. ***D***, GFP-fluorescent cells (indicated by arrows) in striatal sagittal sections from UbGFP:HD94 mice after 3 weeks of acute expression of N-mutHtt. ***i–iii***, Scaled magnifications of the GFP-fluorescent cells shown in ***C***. Scale bar, 50 μm. ***E***, Histogram showing the incidence of GFP-fluorescent cells in the striatum of UbGFP:HD94 mice respect to their UbGFP littermate mice, after 1 to 12 weeks of N-mutHtt expression. ***F***, ***G***, Immunohistochemical detection of GFP in striatal sagittal sections from UbGFP:HD94 mice after 3 weeks of N-mutHtt expression (***G***) and from UbGFP littermates (***F***). Scale bar in ***F*** corresponds to 10 μm in panels ***F–I***. ***H***, ***I***, UbGFP and β-gal colocalization in striatal cells from UbGFP:HD94 mice after 3 weeks of N-mutHtt expression by detection of GFP self-fluorescence (***H***) and immunofluorescence with an anti-β-gal antibody (***I***). ***J***, Western blot showing the full-length reporter construction (Ub^{G76V}-GFP) and the truncated form (GFP), in the striatum of UbGFP and UbGFP:HD94 mice after 1 or 2 weeks of acute expression of N-mutHtt. ***K***, Histogram showing densitometric quantification (in arbitrary units: a.u.) of the full-length reporter construction (Ub^{G76V}-GFP) band corrected by β-actin after 1 or 2 weeks of N-mutHtt expression in UbGFP and UbGFP:HD94 mice.

We then analyzed whether accumulation of Ub^{G76V}-GFP reporter takes place in UbGFP:HD94 mice after acute N-mutHtt expression. Strikingly, with this N-mutHtt expression paradigm we were able for the first time to detect global UPS impairment *in vivo* in a polyQ disease mouse model (Fig. 2*D–I*). Reporter accumulation took place in striatal neurons and was detected only during the first 4 weeks of transgene expression (Fig. 2*D–I*). Double detection of GFP by native fluorescence and of β-gal by immunofluorescence (Fig. 2*H*,*I*) confirmed that the GFP-positive cells were a subset of the neurons just beginning to express the transgene after doxycycline removal.

Despite the limited number of neurons showing accumulation of the Ub^{G76V}-GFP reporter, a modest increase in the level of the reporter was detectable also by Western blot after 1 week of transgene expression (Fig. 2*J*,*K*). Importantly, in view of the recent report of transcriptional effects accounting for increased level of fluorescent UPS reporter proteins in cell lines (Alvarez-Castelao et al., 2009), we performed quantitative RT-PCR analysis of the Ub^{G76V}-GFP reporter transcript. This revealed that the accumulation of the UbG76V-GFP reporter protein is not attributable to transcriptional upregulation because no differences in the level of Ub^{G76V}-GFP reporter transcript were found between UbGFP and UbGFP:HD94 mice after 1 week of acute expression of N-mutHtt (data not shown). Similar to the Western blot data, proteasome activity assays on striatal homogenates showed a trend of decreased caspase-like activity only after 1 week of transgene expression (15.6 ± 18.8% decrease, $p = 0.54$). In the case of chymotrypsin activity, the opposite result (a trend of increased activity) was observed (data not shown), which can be easily explained by the fact that a selective upregulation of this activity is well established in N-mutHtt mouse models (Diaz-Hernandez et al., 2003; Seo et al., 2004; Bett et al., 2006; Seo et al., 2008).

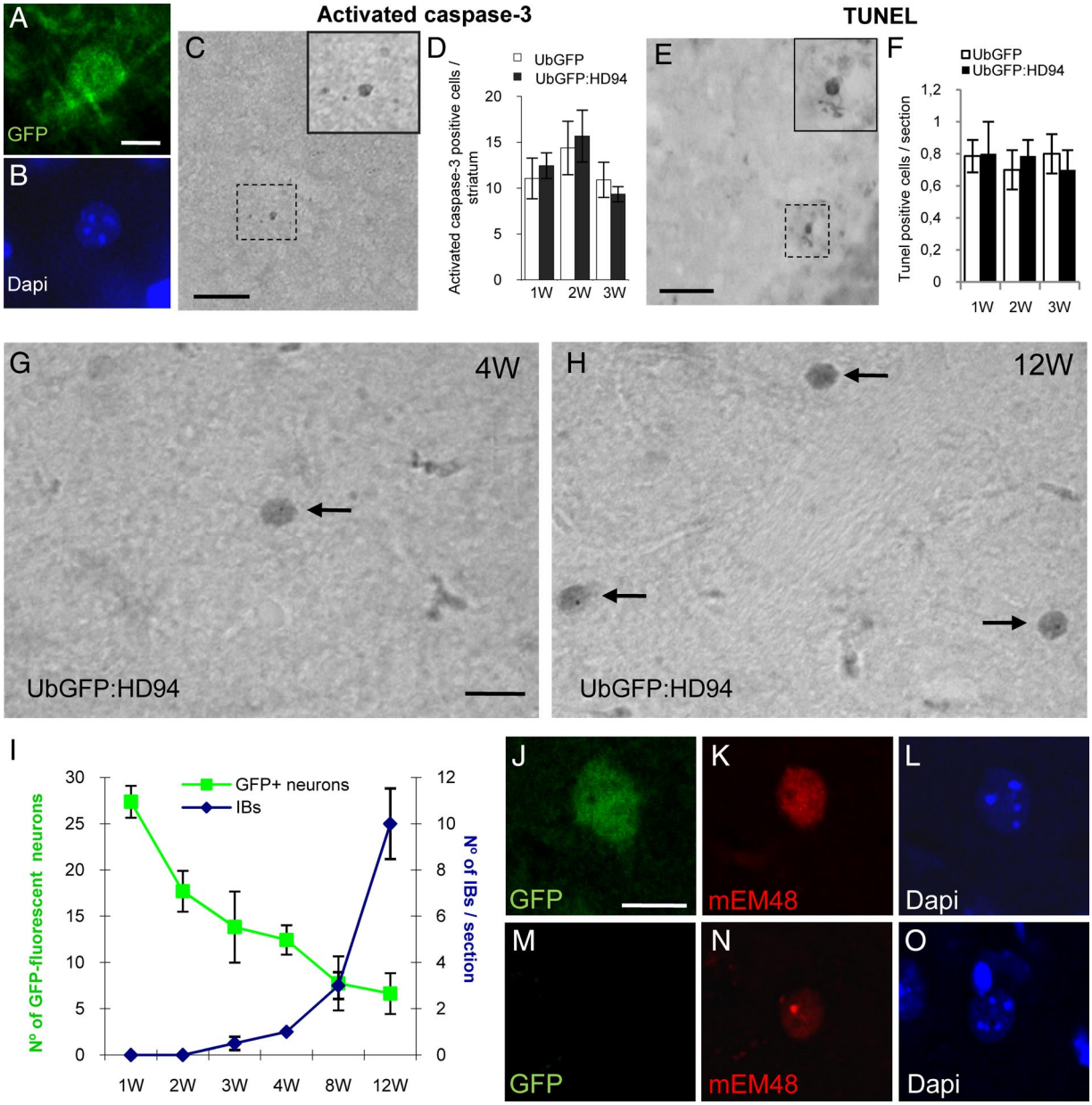

Figure 3. Analysis of apoptosis and of IB formation in the striatum of UbGFP:HD94 mice with acute expression of N-mutHtt. ***A***, ***B***, Fluorescence detection of nuclei with DAPI and of GFP-positive striatal neurons from UbGFP:HD94 mice after 2 weeks of N-mutHtt expression. Scale bar in ***A*** corresponds to 10 μm in ***A***, ***B***. ***C***, Immunohistochemical detection of cleaved caspase-3-positive cells in the striatum of a UbGFP:HD94 mouse after 1 week of N-mutHtt expression. Black delimited image is the magnification of the activated caspase-3-positive cell shown in the punctuated area (***C***). Scale bar, 100 μm. ***D***, Histogram showing the incidence of cleaved caspase-3-immunopositive cells in the striatum of UbGFP:HD94 mice after 1, 2, and 3 weeks of N-mutHtt expression and in their UbGFP littermates. ***E***, TUNEL staining in the striatum of a UbGFP:HD94 mouse after 1 week of N-mutHtt expression. Inset in ***E*** shows a magnification of the TUNEL-positive cell in the boxed area. Scale bar, 100 μm. ***F***, Histogram showing the incidence of TUNEL-positive cells per 30 μm striatal section of UbGFP:HD94 mice after 1, 2, and 3 weeks of N-mutHtt expression, and their UbGFP littermate mice. ***G***, ***H***, Immunohistochemical detection of N-mutHtt-positive cells showing IBs in striatal sagittal sections from UbGFP:HD94 mice after 4 (***G***) and 12 (***H***) weeks of N-mutHtt expression. Scale bar in ***G*** corresponds to 20 μm in ***G*** and ***H***. ***I***, Line chart showing the incidence of GFP-fluorescent cells (green line) and the number of neurons containing IBs (blue line) in striatum of UbGFP:HD94 mice after 1 to 12 weeks N-mutHtt expression. ***J–O***, Confocal images of fluorescence staining with antibodies against GFP (***J***, ***M***) and against N-mutHtt (***K***, ***N***) and DAPI (***L***, ***O***) of striatal sagittal sections from UbGFP:HD94 mice after 4 weeks of N-mutHtt expression. Scale bar in ***J*** corresponds to 10 μm in ***J–O***. Data are presented as the mean ± SEM.

Decrease in Ub^{G76V}-GFP reporter coincides with onset of IB formation

A trivial explanation for the transiency of the detection of cells containing elevated levels of the Ub^{G76V}-GFP reporter is that these cells perish as a result of UPS dysfunction. However, we were unable to detect any nuclear morphologic abnormality in GFP-fluorescent cells indicative of cell death (Fig. 3*A*,*B*). Accordingly, immunohistological staining for markers of apoptosis such as cleaved caspase-3 (Fig. 3*C*,*D*) and TUNEL (Fig. 3*E*,*F*) revealed neither an increase in the number of positive cells in UbGFP:HD94 mice with respect to UbGFP littermates nor colocalization with Ub^{G76V}-GFP.

To explore the possibility that Ub^{G76V}-GFP reporter shutdown correlates with IB formation, we monitored the rate of IB formation by immunohistochemistry with antibodies against N-mutHtt and performed double immunofluorescence detection of N-mutHtt IBs and of native GFP fluorescence. As shown in Figure 3*G–I*, after acute expression of N-mutHtt in UbGFP:

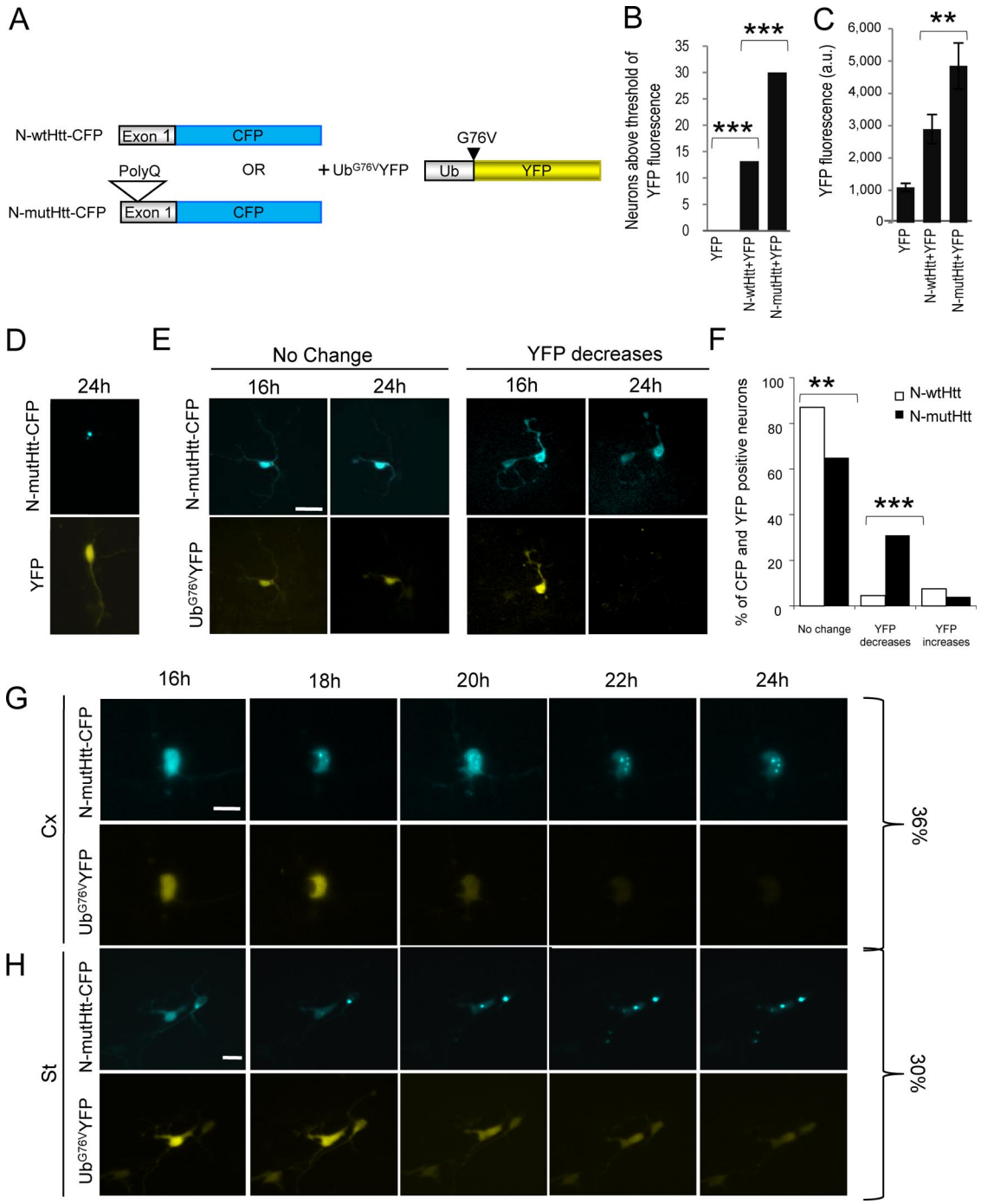

Figure 4. Accumulation of the UPS reporter is also transient in neuronal primary cultures expressing N-mutHtt. ***A***, Diagram of the transfected constructions. Open reading frames of exon 1 and ubiquitin (Ub) are shown in open boxes. An empty triangle indicates where the expanded polyQ tract (94 CAGs) is located. The head arrow indicates the place where the mutation G76V is placed in the reporter construction. CFP and YFP tags are indicated by cyan and yellow boxes, respectively. ***B***, Histogram of average percentage of striatal neurons transfected with Ub^{G76V}YFP (YFP), N-wtHtt-CFP + Ub^{G76V}YFP (N-wtHtt + YFP), or N-mutHtt-CFP + Ub^{G76V}YFP (N-mutHtt + YFP), showing above threshold-yellow fluorescence 16 h after transfection. This histogram does not show error bars because significant differences between groups were evaluated using two proportion comparison test. ***C***, Histogram showing the yellow fluorescence intensity in striatal neurons transfected with YFP, N-wtHtt + YFP, or N-mutHtt + YFP, 16 h after transfection (in arbitrary units of YFP fluorescence). Data are presented as the mean ± SEM. ***D***, Striatal neuron 24 h after transfection with N-mutHtt-CFP + YFP with no degradation signal. ***E***, Striatal neurons transfected with N-mutHtt-CFP + Ub^{G76V}YFP, 16 h or 24 h after transfection. Scale bar, 20 μm. ***F***, Histogram showing average percentage of striatal neurons transfected with N-mutHtt-CFP + Ub^{G76V}YFP (N-mutHtt) (black bars) or N-wtHtt-CFP + Ub^{G76V}YFP (N-wtHtt) (white bars) in which yellow fluorescence does not change, decreases, or increases during the 8 h observation period. This histogram does not show error bars because significant differences between groups were evaluated using two-proportion comparison test. ***G***, ***H***, Cortical (***G***) and striatal (***H***) neurons transfected with N-mutHtt-CFP + Ub^{G76V}YFP in which yellow fluorescence decreases with time. 36% of the cortical transfected neurons and 30% of the striatal transfected neurons build visible IBs, whereas YFP fluorescence decreases with time as shown at 16, 18, 20, 22, and 24 h posttransfection. Scale bars, 15 μm. $^{**}p < 0.005$, $^{***}p < 0.001$).

HD94 mice, IBs are first detected after 4 weeks of transgene expression and coincide with the disappearance of cells with elevated Ub^{G76V}-GFP levels. Interestingly, in the double fluorescence studies, we were unable to detect IBs in the GFP-fluorescent neurons (Fig. 3*J–L*). Likewise, IB-harboring neurons did not show GFP fluorescence (Fig. 3*M–O*) with the exception of a few cells in which faint GFP-fluorescence was restricted to the IBs (data not shown).

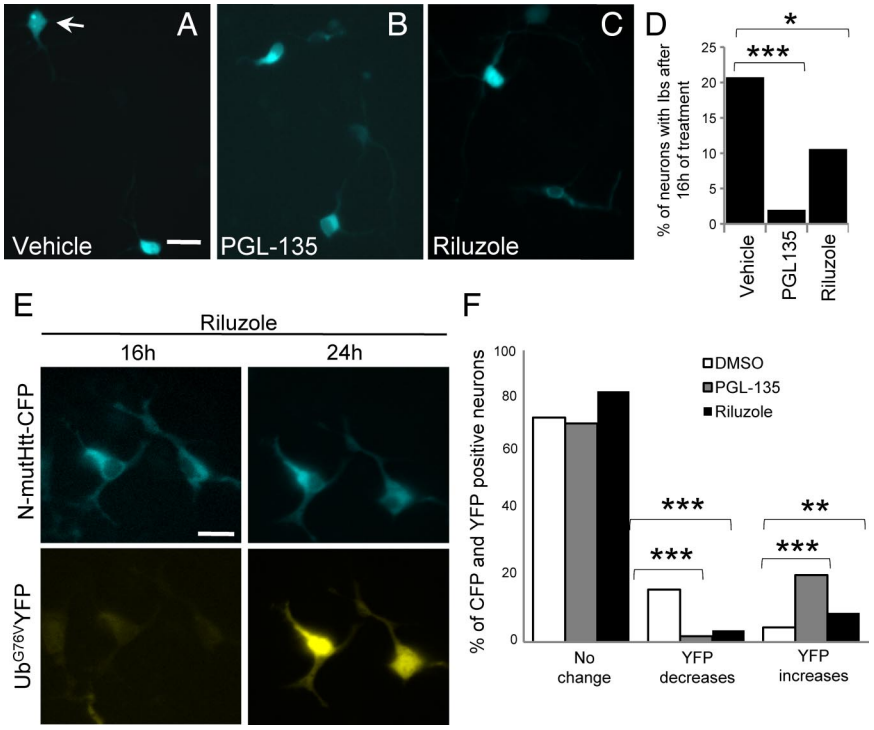

Figure 5. Compunds that inhibit N-mutHtt-aggregation prevent IB formation as well as UPS recovery in neuronal primary cultures. ***A–C***, Cortical neurons transfected with N-mutHtt-CFP + Ub^{G76V}YFP, treated with vehicle (***A***) or the antiaggregation compounds PGL-135 (400 μM) (***B***) or riluzole (40 μM) (***C***). White arrows indicate neurons with IBs. Scale bar in ***A*** corresponds to 10 μm in panels ***A–C***. ***D***, Histogram showing average percentage of cortical neurons transfected with N-mutHtt-CFP + Ub^{G76V}YFP that have IBs after 16 h of incubation with vehicle, PGL-135 (400 μM), or riluzole (40 μM). ***E***, Riluzole (40 μM)-treated neurons showing increased YFP signal between 16 h and 24 h after transfection with N-mutHtt + Ub^{G76V}YFP. Scale bar, 10 μm. ***F***, Histogram showing average percentage of cortical neurons transfected with N-mutHtt-CFP + Ub^{G76V}YFP, treated with vehicle, PGL-135 (400 μM), or riluzole (40 μM), in which yellow fluorescence does not change, decreases, or increases during the 8 h observation period. *$p < 0.05$, **$p < 0.005$, ***$p < 0.001$.

Antiaggregation compounds block IB formation and cause persistent Ub^{G76V}-GFP accumulation in primary cultured neurons

Recovery of UPS function after IB formation has recently been reported in rat striatal primary neurons expressing a different fluorescent UPS reporter, namely mRFP with the CL1 peptide fused to the C terminus (mRFPu) (Mitra et al., 2009). We wondered whether similar results could be obtained with the Ub^{G76V}-based reporter and, more importantly, whether antiaggregation compounds would demonstrate that N-mutHtt aggregation is indeed required for the recovery of the UPS. Mouse striatal and cortical primary neurons were cotransfected with exon 1-encoded N-terminal Htt with 16 or 94 glutamines fused to CFP (N-wtHtt-CFP or N-mutHtt-CFP) and with the reporter of UPS activity Ub^{G76V}-YFP (Fig. 4*A*). As shown in Figure 4, *B* and *C*, 16 h after transfection, N-mutHtt-CFP-transfected neuronal cultures showed increased accumulation of the Ub^{G76V}-YFP reporter compared with N-wtHtt-CFP-transfected cells, both in terms of percentage of neurons showing YFP fluorescence (Fig. 4*B*) and in terms of fluorescence intensity (Fig. 4*C*). We then monitored the cultures every two hours between 16 and 24 h posttransfection (Fig. 4*D–G*). During this period of observation, the majority of N-wtHtt-CFP-transfected neurons that showed YFP fluorescence retained the same level of YFP fluorescence. However, in good agreement with the transient Ub^{G76V}-GFP reporter accumulation observed *in vivo* after acute expression of N-mutHtt in UbGFP:HD94 mice, >30% of the N-mutHtt-CFP-transfected neurons that showed YFP fluorescence progressively lost YFP signal along the 8 h observation period, while retaining normal neuronal morphology and constant N-mutHtt-CFP signal. In good agreement with the previous report of recovery of UPS function attributable to IB formation (Mitra et al., 2009), we observed that 36% of the N-mutHtt-CFP-transfected cortical neurons grew visible IBs as YFP signal vanished along the observation period (Fig. 4*F*). Similar results were obtained in striatal neurons (Fig. 4*G*). Importantly, the decrease in YFP signal appeared not to be attributable to sequestration of the YFP reporter into the IBs because no YFP colocalization was observed in the N-mutHtt-CFP-positive IBs. The empty vector with YFP (without degradation signal) was also assayed as an additional control to further rule out capture of the reporter protein into the IBs (Fig. 4*D*).

To further test whether N-mutHtt aggregation and IB formation play a role in the recovery of UPS function, we analyzed the effect of two compounds that prevent N-mutHtt aggregation: riluzole and PGL-135 (Heiser et al., 2002; Hockly et al., 2006). As shown in Figure 5*A–D*, adding 40 μM riluzole or 400 μM PGL-135 to the culture medium immediately after transfection resulted in a dramatic decrease in the percentage of transfected neurons showing IBs 16 h after transfection. Interestingly, the decrease in YFP fluorescence observed between 16 and 24 h posttransfection in a subset of N-mutHtt-CFP + Ub^{G76V}-YFP-transfected neurons was fully precluded by both aggregation inhibitors. Moreover, as a result of these drug treatments we observed an increase in YFP fluorescence in a subset of N-mutHtt-CFP + Ub^{G76V}-YFP-transfected neurons during the 8 h observation period (Fig. 5*E*,*F*).

Treatment with aggregation inhibitors results in robust Ub^{G76V}-GFP reporter accumulation in HD94 and in R6/1 mice

We then decided to extrapolate the antiaggregation compound approach to the mouse model. Because PGL-135 had been reported to be metabolically unstable after *in vivo* administration to mice (Hockly et al., 2006), we decided to establish an acute riluzole administration protocol capable of preventing or delaying the IB formation detected after 4 weeks of N-mutHtt transgene expression in UbGFP:HD94 mice. After 3.5 weeks of transgene expression, UbGFP:HD94 mice were administered different doses of riluzole for 3 d in drinking water. As shown in Figure 6, *A* and *B*, the highest riluzole dose effectively prevented IB formation as evidenced by the dramatically lower number of IBs detected by immunohistochemical analysis with anti-N-terminal Htt in the striatum of riluzole-administered mice compared to the number of IBs in vehicle administered mice (60.2 ± 6.8% decrease, $p < 0.05$). Moreover, when we used the same riluzole administration paradigm in 3-week-old UbGFP:R6/1 mice (the age at which IBs are first detected, after which their numbers increase exponentially), immunohistochemical analysis with

anti-N-terminal Htt antibody revealed that riluzole was also able to prevented IB formation at this stage of R6/1 neuropathology (Fig. 6*D*,*E*) as evidenced by the dramatically lower number of IBs in riluzole-treated mice as compared to vehicle-treated mice (64.3 ± 25.7% decrease, $p < 0.05$). This reduction in the number of IBs as a consequence of riluzole administration to 3-week-old UbGFP:R6/1 mice was confirmed by a cell sorter-based quantification of IBs in fractions obtained from the brains of vehicle or riluzole treated UbGFP:R6/1 mice that were IB-enriched by magnetic sorting (Fig. 6*E*,*F*). The magnetic sorting-based purification and the cell sorted-based quantification were performed according to the previously described method (Diaz-Hernandez et al., 2006). Finally, the diminished load of IBs as a consequence of riluzole administration was also confirmed by the filter-trap assay (Fig. 6*G*). To rule out the possibility that the observed reduction in IB load was attributable to a riluzole-mediated decrease in N-terminal Htt expression, we performed Western blot (Fig. 6*H*) and quantitative RT-PCR analysis of N-terminal Htt and found no effect of riluzole on the expression of N-terminal Htt.

If N-mutHtt aggregation and subsequent IB formation is the reason why Ub^{G76V}-GFP reporter accumulates only transiently after acute expression in adult UbGFP:HD94 mice and why it does not accumulate in constitutively expressing UbGFP:HD94 or even UbGFP:R6/1 mice (Maynard et al., 2009), riluzole administration should boost reporter accumulation when administered at the time of IB formation in any of these models. To test this, we first verified that riluzole administration did not affect expression of the Ub^{G76V}-GFP reporter in UbGFP singly transgenic control mice. This was confirmed by Western blot (Fig. 7*A*) and by quantitative RT-PCR (data not shown). Accordingly, as shown in Figure 7, *D–F* and *I*, riluzole administration did not affect immunohistochemical detection of Ub^{G76V}-GFP reporter in UbGFP singly transgenic control mice. However, riluzole administration to 3.5 weeks ON UbGFP:HD94 mice did result in a significant 420 ± 28.6% ($p < 0.05$) increase in the number of Ub^{G76V}-GFP-positive cortical neurons (Fig. 7*C*). The observed increase in Ub^{G76V}-GFP-positive striatal neurons, however, did not reach significance, probably because of the limited number of neurons showing transgene expression at this time of induction in the

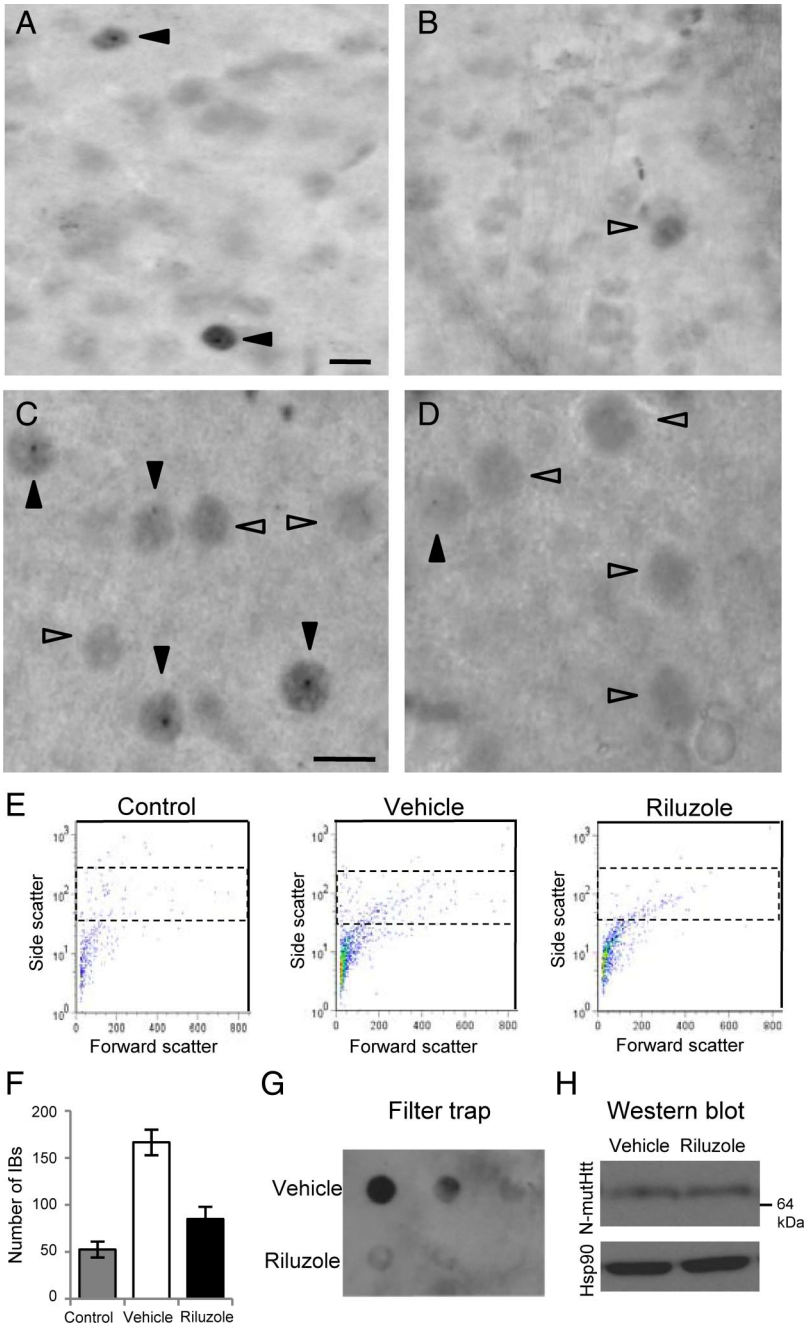

Figure 6. Effect of riluzole treatment *in vivo* on IB formation in UbGFP:HD94 and UbGFP:R6/1 mice. Riluzole was administered for 3 d in the drinking water. The highest tested dose was 2 g/L for the first day and, in view of the hypoactivity induced in both control and transgenic mice, it was decreased to 1.2 g/L for the second and third days. This resulted in decreased IB formation both in 3-month-old UbGFP:HD94 mice after 3.5 weeks of acute expression of N-mutHtt and in 3-week-old UbGFP:R6/1 mice. ***A–D***, Immunohistochemical analysis of striatal neurons from 3-month-old UbGFP:HD94 mice after 3.5 weeks of acute expression of N-mutHtt (***A***, ***B***) or 3-week-old UbGFP:R6/1 mice (***C***, ***D***), after 3 d of treatment with vehicle (***A***, ***C***) or riluzole (***B***, ***D***), with an antibody that recognizes N-mutHtt. Full head arrows indicate neurons with IBs, empty head arrows indicate diffuse N-mutHtt staining. Scale bar in ***A*** corresponds to 10 μm in panels ***A*** and ***B***, scale bar in ***C*** corresponds to 10 μm in ***C*** and ***D***. ***E***, IB-enriched fractions obtained by magnetic sorting from brain of vehicle- or riluzole-treated UbGFP:R6/1 mice were analyzed in a flow cytometer. Control panel shows background corresponding to the magnetic beads and the detecting antibodies (with PBS instead of IB-enriched brain fractions). Graphs show the number and complexity of particles present in the sorted fractions. ***F***, Histogram showing the quantification of particles detected by flow cytometry in the region with complexity (side scatter) and size (forward scatter) where IBs are known to be present (boxed in the graphs in ***G***). ***G***, Filter retardation assay for detection of N-mutHtt containing aggregates from three vehicle- and three riluzole-treated R6/1 mice (3 weeks old). Membrane was probed with the N-mutHtt antibody. ***H***, Western blot showing level of soluble N-mutHtt in the striatum of 3-week-old R6/1 mice treated with vehicle or riluzole.

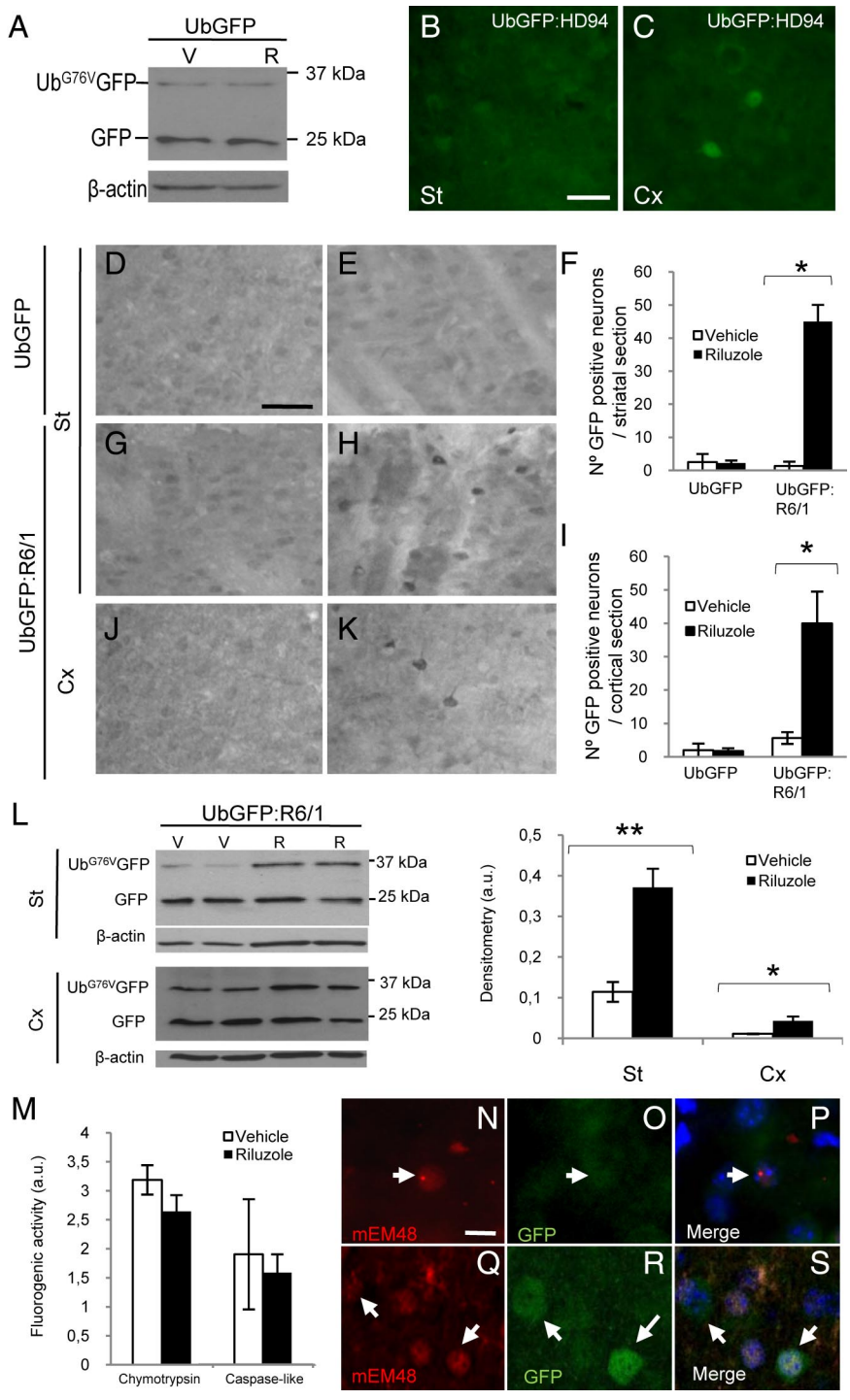

Figure 7. Antiaggregation treatment prevents UPS recovery *in vivo* in UbGFP:HD94 and UbGFP:R6/1 mice. ***A***, Western blot showing detection of the Ub ^{G76V}-GFP reporter in the striatum of UbGFP mice treated with vehicle (V) or riluzole (R) (first day 2 g/L and the rest at 1.2 g/L) corrected by β-actin. ***B***, ***C***, GFP-fluorescence detection in striatal (St, ***B***) and cortical (Cx, ***C***) sagittal sections from UbGFP:HD94 mice treated for 3 d with riluzole after 4 weeks of acute expression of N-mutHtt. Scale bar in ***B*** corresponds to 20 μm in ***B*** and ***C***. ***D***, ***E***, ***G***, ***H***, ***J***, ***K***, Immunohistochemical detection of GFP in striatal (***D***, ***E***, ***G***, ***H***) or cortical (***J***, ***K***) sagittal sections from 3-week-old UbGFP (***D***, ***E***) or UbGFP:R6/1 (***G***, ***H***, ***J***, ***K***) mice after the 3 d vehicle (***D***, ***G***, ***J***) or riluzole (***E***, ***H***, ***K***) administration. Scale bar in ***D*** corresponds to 50 μm in panels ***D***, ***E***, ***G***, ***H***, ***J***, and ***K***. ***F***, ***I***, Histograms showing the number of GFP-positive neurons in striatal (***F***) or cortical (***I***) sagittal sections of UbGFP:R6/1 or UbGFP mice treated with vehicle or riluzole. ***L***, Western blot showing the full-length reporter protein (Ub ^{G76V}-GFP) and the truncated form (GFP), in striatum (St) or cortex (Cx) of UbGFP:R6/1 mice treated with vehicle (V) or riluzole (R); and histogram showing the densitometric quantification (in arbitrary units: a.u.) of Ub ^{G76V}-GFP corrected with respect to β-actin. ***M***, Histogram showing the chymotrypsin-like and caspase-like peptidase activities of the proteasome (by determining cleavage of the fluorogenic substrates SUC-LLVY-AMC and Z-LLE-β-NAP, respectively) assayed in striatal extracts from 3-week-old U1R6/1 mice treated with vehicle or riluzole. ***N–S***, Confocal images of fluorescence staining with antibodies against N-mutHtt (red) and GFP (green) and with DAPI (blue) of striatal sagittal sections from 3-week-old UbGFP:R6/1 mice treated with vehicle (***N–P***) or riluzole (***Q–S***). Scale bar in ***N*** corresponds to 10 μm in ***N–S***. Data are presented as mean $\pm$ SEM. *$p < 0.05$; **$p < 0.005$.

conditional model (Fig. 7*B*). Strikingly, when riluzole was administered to 3-week-old UbGFP:R6/1 mice, a dramatic increase in the number of Ub ^{G76V}-GFP reporter-positive cells was observed both in striatum and cortex (Fig. 7*D–K*). Given the widespread accumulation of Ub ^{G76V}-GFP reporter in riluzole-administered UbGFP:R6/1 mice, we decided to analyze the level of Ub ^{G76V}-GFP also by Western blot. As shown in Figure 7*L*, significant 326 $\pm$ 41% ($p < 0.005$) and 388 $\pm$ 100% ($p < 0.05$) increases in striatal and cortical Ub ^{G76V}-GFP levels, respectively, were observed in riluzole-treated mice compared to vehicle-treated mice. However, when we analyzed proteasome activity in striatal homogenates from vehicle- and riluzole-administered UbGFP:R6/1 mice, only a trend toward decreased activity was observed in riluzole treated mice (Fig. 7*M*). As shown in Figure 7*N–S*, immunohistological analysis confirmed that riluzole administration efficiently reduced IB load in UbGFP:R6/1 mice and that Ub ^{G76V}-GFP reporter-positive cells showed only diffuse N-mutHtt staining. In summary, as we have recently demonstrated (Maynard et al., 2009), UbGFP:R6/1 mice do not show accumulation of the UPS impairment reporter under normal conditions. However, UPS impairment does indeed occur when IB formation is prevented by an aggregation inhibitor.

Discussion

By combining UPS reporter mice with an inducible mouse model of HD, we demonstrate, for the first time, polyQ-induced global UPS impairment *in vivo*. This occurred in adult neurons as a consequence of acute expression of N-mutHtt and lasted only transiently until IBs became readily detectable. Furthermore, with the use of antiaggregation compounds in both cell and animal models, we were able demonstrate that aggregate formation is indeed responsible for UPS recovery.

Neurodegenerative disorders are characterized by the presence of intracellular ubiquitylated inclusions (Bossy-Wetzel et al., 2004). This, combined with the role of the UPS in protecting the intracellular environment from abnormal and potentially hazardous proteins (Glickman and Ciechanover, 2002), has given rise to the hypothesis that UPS impairment underlies neurodegenerative processes (Ciechanover and Brundin, 2003). However, exploring this hypothesis has been often limited by technical issues (Hernández et al., 2004; Ortega et al., 2007). Particularly, answering the question of whether the PolyQ mutant proteins induce UPS impairment has been

difficult, in light of the discrepancy between results obtained from cell and mouse models (Davies et al., 2007; Ortega et al., 2007).

The results reported here clarify that expression of N-mutHtt does have the potential to induce UPS impairment *in vivo* in mouse models, thus fitting with previous observations in cell models expressing fluorescent UPS reporter proteins (Bence et al., 2001; Jana et al., 2001; Bennett et al., 2005; Duennwald and Lindquist, 2008; Mitra et al., 2009). However, N-mutHtt-induced UPS impairment *in vivo* is transient and, in good agreement with previous reports combining PolyQ mouse models with the same (Bowman et al., 2005; Maynard et al., 2009) or similar (Bett et al., 2009) reporter mice, it is not detected with constitutive N-mutHtt expression in adult mice. Finally, that aggregate formation correlates with UPS recovery had also been recently reported in a cell model (Mitra et al., 2009), and here we were able to demonstrate causality with the use of antiaggregation compounds in a cell model and also *in vivo* in mouse models.

Regarding the proposed role of IBs in the recovery of an altered UPS, it could be argued that fluorescence experiments do not rule out that inclusions sequester the UFD substrate and thus reduce its detectable fluorescence. However, in such case, one would expect some YFP reporter fluorescence colocalization in the growing IBs. Similarly, detection of cells with a faint GFP fluorescence restricted to the IBs in UbGFP:HD94 mice after acute expression of N-mutHtt is also a very rare event. Furthermore, sequestration of proteins with a fluorescent-protein tag into IBs does not preclude detection of the fluorescent protein as is clearly evidenced here by the detection of N-mut-Htt-CFP in the IBs and in similar results obtained with versions of mut-Htt fused to GFP (Arrasate et al., 2004) or YFP (Chandra et al., 2008).

Our results are consistent not only with the above-mentioned studies based on the use of fluorescent UPS reporter proteins, but also with studies based on analysis of proteasome enzymatic activity (e.g., by the use of small fluorogenic substrates). For example, it had been shown that 26S proteasome activity decreases in the presence of ubiquitylated filamentous microaggregates purified from HD mice, whereas purified IBs on the other hand did not show any such inhibitory effect (Diaz-Hernandez et al., 2004; Diaz-Hernandez et al., 2006). Similarly, proteasome activity was not reduced in brain homogenates of adult HD mice in which IBs are readily detectable (Diaz-Hernandez et al., 2003; Bett et al., 2006). Our finding of IB formation correlating with restoration of UPS function supports the notion that formation of IBs has a beneficial effect by sequestering the smaller and more toxic species of N-mutHtt. This fits with the previously suggested general protective role of IBs in HD cell models (Arrasate et al., 2004) and, more specifically, with respect to UPS function (Mitra et al., 2009).

If, as suggested, oligomeric mutant Htt species are in fact the species that disrupt the UPS, a possible mechanism could be a direct interaction of ubiquitylated microaggregates with the 19S particles of 26S proteasomes. It is well known that the 19S particles recognize poly-ubiquitin motifs and that the ATPases in the 19S particles then open the gate of the 20S core particle to allow entry of the unfolded substrate (Kohler et al., 2001; Smith et al., 2007). We also previously showed by immuno-electron microscopy a direct interaction of mutant Htt filaments with the 19S caps of 26 proteasomes (Diaz-Hernandez et al., 2006). It is therefore possible that after interaction with a ubiquitylated microaggregate, given the size and tight aggregation of the microaggregate, the 19S particle is not able to unfold the aggregate particle to induce the opening of the gate. Regarding the mechanism for recovery, it is possible that after encountering an increase in the cellular load of poly-ubiquitylated conjugates, the cell triggers the aggresome-forming response (Kopito, 2000; Sherman and Goldberg, 2001). Consequently, the microtubule-mediated transport of microaggregates dispersed throughout the cell toward the microtubule organizing center (MTOC) (Johnston et al., 1998; Muchowski et al., 2002) would result in decreased concentration of ubiquitylated microaggregates in the cell, and subsequent UPS recovery, in a time frame similar to that required for detection of IBs.

The protective role of soluble and/or microaggregated N-mutHtt sequestration into IBs may also explain why adenoviral expression of a GFPu reporter in R6/2 mice did not detect accumulation in cell bodies of neurons while it was able to detect accumulation in synaptic terminals (Wang et al., 2008). Because sequestration of soluble and/or microaggregated N-mutHtt into IBs involves transport along the microtubule network (Kopito, 2000; Muchowski et al., 2002), the local concentration of soluble and/or microaggregated N-mutHtt may be higher in the synaptic terminals because of less efficient removal by the microtubule network in the synaptic terminal.

The same reporter mice that were applied in our study have confirmed UPS dysfunction in prion-infected mice (Kristiansen et al., 2007) and in transgenic mice overexpressing a mutant form of SOD1 that is responsible for familial amyotrophic lateral sclerosis (Cheroni et al., 2009). In contrast, HD mice failed to show accumulation of reporter proteins (Bett et al., 2009; Maynard et al., 2009) even in late stages of the disease when an age-dependent decrease in proteasome activity has taken place (this study). Furthermore, in mouse models of two additional PolyQ diseases, namely SCA7 (Bowman et al., 2005) and spinal and bulbar muscular atrophy (Tokui et al., 2009) combined with the same reporter mice, the UPS remains operative. Thus it appears that the UPS manages to escape global UPS impairment in the face of a chronic pathological polyQ challenge, possibly via efficient sequestration of the toxic polyQ species into IBs.

It should be noted, however, that the use of fluorescent reporter proteins as the main approach to assess UPS functions, like any of the currently available techniques, has limitations. For instance, we have shown here that the Ub-GFP reporter is sensitive enough to accumulate when a 40% decrease in proteasome chymotrypsin activity, as measured with fluorogenic substrates, has taken place, but it would not detect more subtle impairments at the level of proteasome endoproteolytic activity. The use of fluorogenic substrates, on the other hand, is a poor indicator of the functionality of the UPS as it is not clear how it reflects the capacity of the 26S to degrade ubiquitylated proteins and because, unlike the use of fluorescent reporter proteins, it would fail to detect impairments taking place only in a subset of cells of the analyzed tissue. Therefore, caution is recommended when inferring suggestive or definitive conclusions from these kind of studies in view of the intrinsic weaknesses of each approach.

In summary, our results finally reconcile the data from cell models supporting polyQ-induced UPS impairment with the contradictory findings of no impairment in mouse models. More specifically, our results demonstrate that N-mutHtt can indeed impair UPS function *in vivo* as evidenced by the accumulation of the Ub-GFP reporter protein in the brain of HD mice but also that this occurs only transiently because of the protective effect of N-mutHtt aggregation. Our work also exemplifies the robustness of the UPS even at late stages of disease in HD mice, thus suggesting that this proteolytic machinery could be exploited to reduce the load of toxic proteins in HD and related disorders.

References

Alvarez-Castelao B, Martin-Guerrero I, Garcia-Orad A, Castano JG (2009) Cytomegalovirus promoter up-regulation is the major cause of increased protein levels of unstable reporter proteins after treatment of living cells with proteasome inhibitors. J Biol Chem 284:28253–28262.

Arrasate M, Mitra S, Schweitzer ES, Segal MR, Finkbeiner S (2004) Inclusion body formation reduces levels of mutant huntingtin and the risk of neuronal death. Nature 431:805–810.

Bence NF, Sampat RM, Kopito RR (2001) Impairment of the ubiquitin-proteasome system by protein aggregation. Science 292:1552–1555.

Bennett EJ, Bence NF, Jayakumar R, Kopito RR (2005) Global impairment of the ubiquitin-proteasome system by nuclear or cytoplasmic protein aggregates precedes inclusion body formation. Mol Cell 17:351–365.

Bennett EJ, Shaler TA, Woodman B, Ryu KY, Zaitseva TS, Becker CH, Bates GP, Schulman H, Kopito RR (2007) Global changes to the ubiquitin system in Huntington's disease. Nature 448:704–708.

Bett JS, Goellner GM, Woodman B, Pratt G, Rechsteiner M, Bates GP (2006) Proteasome impairment does not contribute to pathogenesis in R6/2 Huntington's disease mice: exclusion of proteasome activator REG-gamma as a therapeutic target. Hum Mol Genet 15:33–44.

Bett JS, Cook C, Petrucelli L, Bates GP (2009) The ubiquitin-proteasome reporter GFPu does not accumulate in neurons of the R6/2 transgenic mouse model of Huntington's disease. PLoS One 4:e5128.

Bossy-Wetzel E, Schwarzenbacher R, Lipton SA (2004) Molecular pathways to neurodegeneration. Nat Med 10 [Suppl]:S2–S9.

Bowman AB, Yoo SY, Dantuma NP, Zoghbi HY (2005) Neuronal dysfunction in a polyglutamine disease model occurs in the absence of ubiquitin-proteasome system impairment and inversely correlates with the degree of nuclear inclusion formation. Hum Mol Genet 14:679–691.

Chandra S, Shao J, Li JX, Li M, Longo FM, Diamond MI (2008) A common motif targets huntingtin and the androgen receptor to the proteasome. J Biol Chem 283:23950–23955.

Cheroni C, Marino M, Tortarolo M, Veglianese P, De Biasi S, Fontana E, Zuccarello LV, Maynard CJ, Dantuma NP, Bendotti C (2009) Functional alterations of the ubiquitin-proteasome system in motor neurons of a mouse model of familial amyotrophic lateral sclerosis. Hum Mol Genet 18:82–96.

Ciechanover A, Brundin P (2003) The ubiquitin proteasome system in neurodegenerative diseases: sometimes the chicken, sometimes the egg. Neuron 40:427–446.

Cook C, Petrucelli L (2009) A critical evaluation of the ubiquitin-proteasome system in Parkinson's disease. Biochim Biophys Acta 1792:664–675.

Davies JE, Sarkar S, Rubinsztein DC (2007) The ubiquitin proteasome system in Huntington's disease and the spinocerebellar ataxias. BMC Biochem 8 [Suppl 1]:S2.

Davies SW, Sathasivam K, Hobbs C, Doherty P, Mangiarini L, Scherzinger E, Wanker EE, Bates GP (1999) Detection of polyglutamine aggregation in mouse models. Methods Enzymol 309:687–701.

Diaz-Hernandez M, Hernandez F, Martin-Aparicio E, Gomez-Ramos P, Moran MA, Castano JG, Ferrer I, Avila J, Lucas JJ (2003) Neuronal induction of the immunoproteasome in Huntington's disease. J Neurosci 23:11653–11661.

Diaz-Hernandez M, Moreno-Herrero F, Gomez-Ramos P, Moran MA, Ferrer I, Baro AM, Avila J, Hernandez F, Lucas JJ (2004) Biochemical, ultrastructural, and reversibility studies on huntingtin filaments isolated from mouse and human brain. J Neurosci 24:9361–9371.

Diaz-Hernandez M, Torres-Peraza J, Salvatori-Abarca A, Moran MA, Gomez-Ramos P, Alberch J, Lucas JJ (2005) Full motor recovery despite striatal neuron loss and formation of irreversible amyloid-like inclusions in a conditional mouse model of Huntington's disease. J Neurosci 25:9773–9781.

Diaz-Hernandez M, Valera AG, Moran MA, Gomez-Ramos P, Alvarez-Castelao B, Castano JG, Hernandez F, Lucas JJ (2006) Inhibition of 26S proteasome activity by huntingtin filaments but not inclusion bodies isolated from mouse and human brain. J Neurochem 98:1585–1596.

Dubinsky JM (1989) Development of inhibitory synapses among striatal neurons in vitro. J Neurosci 9:3955–3965.

Duennwald ML, Lindquist S (2008) Impaired ERAD and ER stress are early and specific events in polyglutamine toxicity. Genes Dev 22:3308–3319.

Glickman MH, Ciechanover A (2002) The ubiquitin-proteasome proteolytic pathway: destruction for the sake of construction. Physiol Rev 82:373–428.

Heiser V, Engemann S, Brocker W, Dunkel I, Boeddrich A, Waelter S, Nordhoff E, Lurz R, Schugardt N, Rautenberg S, Herhaus C, Barnickel G, Bottcher H, Lehrach H, Wanker EE (2002) Identification of benzothiazoles as potential polyglutamine aggregation inhibitors of Huntington's disease by using an automated filter retardation assay. Proc Natl Acad Sci U S A 99 [Suppl 4]:16400–16406.

Hernández F, Díaz-Hernández M, Avila J, Lucas JJ (2004) Testing the ubiquitin–proteasome hypothesis of neurodegeneration in vivo. Trends Neurosci 27:66–70.

Hershko A, Ciechanover A (1998) The ubiquitin system. Annu Rev Biochem 67:425–479.

Hockly E, Tse J, Barker AL, Moolman DL, Beunard JL, Revington AP, Holt K, Sunshine S, Moffitt H, Sathasivam K, Woodman B, Wanker EE, Lowden PA, Bates GP (2006) Evaluation of the benzothiazole aggregation inhibitors riluzole and PGL-135 as therapeutics for Huntington's disease. Neurobiol Dis 21:228–236.

Huettner JE, Baughman RW (1986) Primary culture of identified neurons from the visual cortex of postnatal rats. J Neurosci 6:3044–3060.

Jana NR, Zemskov EA, Wang G, Nukina N (2001) Altered proteasomal function due to the expression of polyglutamine-expanded truncated N-terminal huntingtin induces apoptosis by caspase activation through mitochondrial cytochrome c release. Hum Mol Genet 10:1049–1059.

Johnston JA, Ward CL, Kopito RR (1998) Aggresomes: a cellular response to misfolded proteins. J Cell Biol 143:1883–1898.

Keller JN, Huang FF, Markesbery WR (2000a) Decreased levels of proteasome activity and proteasome expression in aging spinal cord. Neuroscience 98:149–156.

Keller JN, Hanni KB, Markesbery WR (2000b) Possible involvement of proteasome inhibition in aging: implications for oxidative stress. Mech Ageing Dev 113:61–70.

Kohler A, Cascio P, Leggett DS, Woo KM, Goldberg AL, Finley D (2001) The axial channel of the proteasome core particle is gated by the Rpt2 ATPase and controls both substrate entry and product release. Mol Cell 7:1143–1152.

Kopito RR (2000) Aggresomes, inclusion bodies and protein aggregation. Trends Cell Biol 10:524–530.

Kristiansen M, Deriziotis P, Dimcheff DE, Jackson GS, Ovaa H, Naumann H, Clarke AR, van Leeuwen FW, Menendez-Benito V, Dantuma NP, Portis JL, Collinge J, Tabrizi SJ (2007) Disease-associated prion protein oligomers inhibit the 26S proteasome. Mol Cell 26:175–188.

Lindsten K, Menendez-Benito V, Masucci MG, Dantuma NP (2003) A transgenic mouse model of the ubiquitin/proteasome system. Nat Biotechnol 21:897–902.

Mangiarini L, Sathasivam K, Seller M, Cozens B, Harper A, Hetherington C, Lawton M, Trottier Y, Lehrach H, Davies SW, Bates GP (1996) Exon 1 of the HD gene with an expanded CAG repeat is sufficient to cause a progressive neurological phenotype in transgenic mice. Cell 87:493–506.

Martin-Aparicio E, Yamamoto A, Hernandez F, Hen R, Avila J, Lucas JJ (2001) Proteasomal-dependent aggregate reversal and absence of cell death in a conditional mouse model of Huntington's disease. J Neurosci 21:8772–8781.

Mayford M, Bach ME, Huang YY, Wang L, Hawkins RD, Kandel ER (1996) Control of memory formation through regulated expression of a CaMKII transgene. Science 274:1678–1683.

Maynard CJ, Bottcher C, Ortega Z, Smith R, Florea BI, Diaz-Hernandez M, Brundin P, Overkleeft HS, Li JY, Lucas JJ, Dantuma NP (2009) Accumulation of ubiquitin conjugates in a polyglutamine disease model occurs without global ubiquitin/proteasome system impairment. Proc Natl Acad Sci U S A 106:13986–13991.

Mitra S, Tsvetkov AS, Finkbeiner S (2009) Single neuron ubiquitin-proteasome dynamics accompanying inclusion body formation in Huntington disease. J Biol Chem 284:4398–4403.

Muchowski PJ, Ning K, D'Souza-Schorey C, Fields S (2002) Requirement of an intact microtubule cytoskeleton for aggregation and inclusion body formation by a mutant huntingtin fragment. Proc Natl Acad Sci U S A 99:727–732.

Orr HT, Zoghbi HY (2007) Trinucleotide repeat disorders. Annu Rev Neurosci 30:575–621.

Ortega Z, Diaz-Hernandez M, Lucas JJ (2007) Is the ubiquitin-proteasome system impaired in Huntington's disease? Cell Mol Life Sci 64:2245–2257.

Paxinos G, Franklin KBJ (2001) The mouse brain in stereotaxic coordinates, Ed 2. New York; Academic.

Ross CA (1997) Intranuclear neuronal inclusions: a common pathogenic mechanism for glutamine-repeat neurodegenerative diseases? Neuron 19:1147–1150.

Ross CA, Poirier MA (2004) Protein aggregation and neurodegenerative disease. Nat Med 10 [Suppl]:S10–S17.

Seo H, Sonntag KC, Isacson O (2004) Generalized brain and skin proteasome inhibition in Huntington's disease. Ann Neurol 56:319–328.

Seo H, Kim W, Isacson O (2008) Compensatory changes in the ubiquitin-proteasome system, brain-derived neurotrophic factor and mitochondrial complex II/III in YAC72 and R6/2 transgenic mice partially model Huntington's disease patients. Hum Mol Genet 17:3144–3153.

Sherman MY, Goldberg AL (2001) Cellular defenses against unfolded proteins: a cell biologist thinks about neurodegenerative diseases. Neuron 29:15–32.

Smith DM, Chang SC, Park S, Finley D, Cheng Y, Goldberg AL (2007) Docking of the proteasomal ATPases' carboxyl termini in the 20S proteasome's alpha ring opens the gate for substrate entry. Mol Cell 27:731–744.

Tokui K, Adachi H, Waza M, Katsuno M, Minamiyama M, Doi H, Tanaka K, Hamazaki J, Murata S, Tanaka F, Sobue G (2009) 17-DMAG ameliorates polyglutamine-mediated motor neuron degeneration through well-preserved proteasome function in an SBMA model mouse. Hum Mol Genet 18:898–910.

Wang J, Wang CE, Orr A, Tydlacka S, Li SH, Li XJ (2008) Impaired ubiquitin-proteasome system activity in the synapses of Huntington's disease mice. J Cell Biol 180:1177–1189.

Yamamoto A, Lucas JJ, Hen R (2000) Reversal of neuropathology and motor dysfunction in a conditional model of Huntington's disease. Cell 101:57–66.

Zhou H, Cao F, Wang Z, Yu ZX, Nguyen HP, Evans J, Li SH, Li XJ (2003) Huntingtin forms toxic NH2-terminal fragment complexes that are promoted by the age-dependent decrease in proteasome activity. J Cell Biol 163:109–118.